First measurements of ELM ion energies in the ASDEX Upgrade far SOL

M. Kočan, A. Herrmann, H. W. Müller, V. Rohde, T. Eich, M. Bernert, S. Carpentier-Chouchana[1], J. P. Gunn[2], A. Kirk[3], M. Komm[4], R. A. Pitts[1] and ASDEX Upgrade team

Max-Planck-Institut für Plasmaphysik, Bolzmannstr. 2, D-85748 Garching, Germany

[1] ITER Organization, Route de Vinon, CS 90 046, 13067 Saint Paul Lez Durance Cedex, France

[2] CEA, IRFM, F-13108 Saint-Paul-lez-Durance, France

[3] EURATOM/CCFE Fusion Association, Culham Science Centre, Abingdon, Oxon OX14 3DB, UK

[4] Association Euratom-IPP.CR, Institute of Plasma Physics, Za Slovankou 3, 18200 Prague, Czech Republic

E-mail: martin.kocan@ipp.mpg.de

Abstract. Using the Retarding Field Analyser (RFA) technique, ion energies carried by ELM filaments have been measured for the first time in the far scrape-off layer (SOL) of the ASDEX Upgrade tokamak. Energies, $E_{i\,ELM}$, exceeding 160 eV have been found, 5 – 6 cm outside the separatrix, with a decay length of about 2 cm. The measured ELM particle ion temperature in the far SOL is in the range $T_{i\,ELM} \approx 50-80$ eV, in good agreement with the predictions from two simple collisionless models of ELM parallel transport. In between ELMs, $T_i \approx T_e \approx 10$ eV is observed in the far SOL, consistent with relatively strong ion-electron thermal coupling in this region.

PACS: 52.25.Fi, 52.25.Xz, 52.40.Hf, 52.55.Fa, 52.65.-y, 52.70.Ds

1. Introduction

Thermal heat loads to the first wall during edge localized modes (ELMs) have been identified as one of the important issues for ITER burning plasma operation and determine the design of the ITER blanket module shaping and power handling capacity [1]. These heat loads scale with the energies carried by ELM ions to the first wall, which, in turn, depend on dissipation by parallel losses of the ELM energy to the divertor targets as the ELM particles travel across the SOL. Direct measurements of the ELM ion energies in the far SOL are, therefore, important in order to constrain the models of the ELM parallel transport in the SOL [2, 3], which, in turn, increases the confidence in the model predictions towards ITER.

Earlier measurements of the heat loads to the first wall in ASDEX Upgrade (AUG) revealed that up to ~25% of the energy lost per ELM can be deposited on non-divertor components, indicating that ELM ions can carry relatively large fractions of the energy with which they are released into the SOL to the first wall [4, 5, 6]. These observations (also seen later on JET [7, 8]), were consistent with increase by an order of magnitude of the tungsten influx from the outboard limiters in AUG during ELMs compared to inter-ELM periods [9]. Energetic ELM ions (impact energies exceeding 400 eV) in the far SOL (typically 2-3 characteristic SOL power widths outside the separatrix) were measured directly for the first time in JET [10] (and more recently in MAST [11]) using a Retarding Field

Analyzer (RFA) technique. The RFA data in JET was found to be in satisfactory agreement with a fluid model of parallel energy loss along ELM filaments assumed to be propagating across the SOL with specified radial speed [2, 10, 12]. The same model predicts average ELM ion impact energies in the range of 1 keV at the point of first impact with ITER main chamber structures [2, 12], rising concerns about a significant lifetime reduction of the ITER first wall by unmitigated ELMs [1].

This paper describes the first measurements of ELM ion energies in the far SOL of AUG using a new RFA and applying a similar approach to that adopted in [10]. Both, far SOL ELM ($T_{i\,ELM}$) and the inter-ELM (T_i) ion temperatures, are estimated for the first time from the RFA measurements. The experimental $T_{i\,ELM}$ are confronted with the predictions of two models of the ELM parallel transport in the SOL.

2. Experimental results

2.1. Retarding field analyzer

As shown in figure 1, in AUG, the RFA is mounted on a fast horizontal reciprocating drive located on the low field side, 31 cm above the machine equatorial plane at the toroidal angle $\phi = 124°$. The reciprocating system allows the probe to be maintained at a specific position for a user-defined time interval in order to make measurements at fixed radius. Uncertainties in the separatrix and the probe positions lead to ~0.5 cm uncertainty in the probe-separatrix distance, Δr_{sep}.

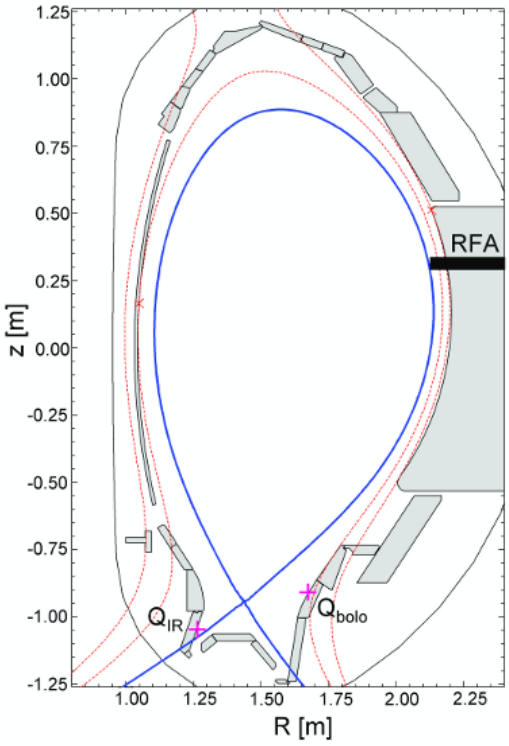

Figure 1. *Poloidal plasma cross-section of the AUG discharge #25773 during the RFA reciprocation. Full line: separatrix, dotted lines: shadow of the outboard and the inboard limiters. RFA is mounted on a fast horizontal reciprocating drive located on the low field side, 31 cm above the machine equatorial plane Also indicated are the positions of the measurements of the power densities by a bolometric diode and the IR camera, used as ELM markers.*

The design of the RFA used in AUG is similar to that employed previously on Tore Supra and much earlier in JET, described in detail elsewhere [13, 14, 15]. The probe head consists of two identical analyzers, aligned parallel to the total magnetic field direction and thus sampling plasma from both directions along the magnetic field lines (referred to as “parallel” direction throughout this paper). The side of the RFA intercepting magnetic field lines coming from the low field side (high

field side) is referred to as LFS (HFS). The probe is protected by a graphite housing with the outer diameter $d = 6.2\,\mathrm{cm}$.

As illustrated schematically in figure 2, each analyzer consists of a slit plate, two principal grids and a collector. A rectangular slit (horizontal length $h = 3\,\mathrm{mm}$) is laser cut into the 125 μm thick slit plate. The width of the slit is $w = 35\,\mu\mathrm{m}$ for the LFS analyzer. The slit plate mounted on the HFS analyzer was erroneously fabricated with a wider aperture (94 μm) and is, therefore, characterized by larger relative ion transmission factor ξ_r (Sec. 2.4). However, using particle-in-cell simulations similar to those described in [13] it has been verified that the wider slit does not affect the measurements. A fraction of the incident ion flux is transmitted through the slit. The optical transmission factor of each grid $\xi_{opt} \cong 0.72$. A third grid (not shown in figure 2) is attached to the rear of the slit plate to render the electric field behind the slit entrance as planar as possible.

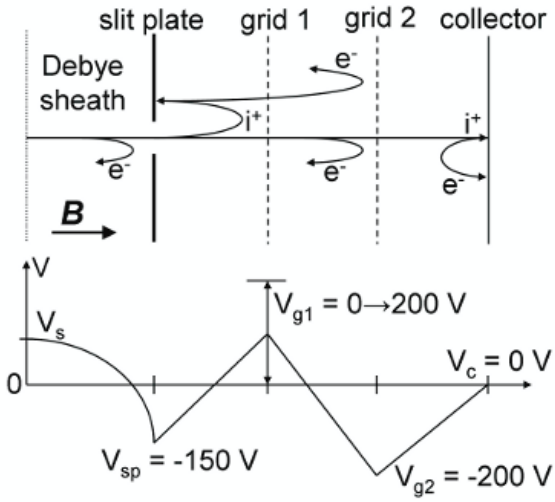

Figure 2. *Schematic of the RFA and the biasing scheme. All voltages refer to torus ground.*

Standard ion retarding bias voltage scheme is applied to both analyzers. Fixed negative voltage is applied to the slit plate ($V_{sp} = -150\,\mathrm{V}$) to measure the ion saturation current i_{sat} as well as to repel most electrons from the incident plasma flux. (In the AUG far SOL, the fast sweeping Langmuir probes (LPs) measure the ELM electron temperature averaged over 25 μs $T_{e\,ELM} \approx 15\,\mathrm{eV}$, with the peaks of $T_{e\,ELM}$ up to 40 eV on unsmoothed signal [16], and the background electron temperature $T_e \approx 10\,\mathrm{eV}$ [17, 18]. However, it should be noticed that none of these scarce T_e measurements are available for the discharge parameters discussed here.) Grid 2 is biased to $V_{g2} = -200$ V to repel the remaining electrons as well as to suppress any secondary electrons emitted inside the analyzer, figure 2. The voltage applied to grid 1, V_{g1}, is swept at 15 Hz from 0 to 200 V. The ion current to the collector (I_c) and i_{sat} are measured at acquisition frequencies of 33 kHz and 2 MHz respectively. The ion saturation current density is derived from i_{sat} as $j_{sat} = i_{sat} / A_{sp}$ with $A_{sp} = 16\,\mathrm{mm}^2$ being the slit plate collecting area. Grid currents are not measured.

In the Debye sheath in front of the RFA all ions are accelerated by $eZ_i(V_s + V_{sp})$, with V_s the sheath potential and Z_i the ion charge, from which eZ_iV_{sp} is removed from them as they proceed the collector (see schematic in figure 2). The energy of collected ions is thus increased by eZ_iV_s compared to their thermal energy at the sheath edge. eZ_iV_s equals to the energy the ions would gain before striking the first wall structure at given radial position. Therefore, the collector signal measured at given Δr_{sep} and V_{g1} indicates that ions would strike the first wall at that radial position with the impact energies $\geq eZ_iV_{g1}$. Note also that no ions are reflected for $V_{g1} \leq V_s$.

2.2. RFA signals during ELMs

These first RFA measurements in AUG were very early on subject to technical difficulties. Breakdowns of the neutral gas inside the analyzer (most likely provoked by enhanced outgassing rates from the RFA internal components during ELMs) partially melted the grids in the early phase of the experiment, excluding normal RFA operation. The only useable data were obtained in a single reciprocation into the deuterium fuelled, single null lower diverted Type-I ELMy H-mode discharge #25773 with $\mathbf{B}\times\nabla B$ pointing downwards (magnetic equilibrium shown in figure 1) for which plasma density $n_e = 7.5\cdot 10^{19}$ m^{-3} (60 % of the Greenwald limit), plasma current $I_p = 1$ MA, toroidal magnetic field $B_t = 2.4$ T, safety factor at the 95% of the flux surface $q_{95} = 4.5$, major radius $R = 1.69$ m, neutral beam and the ohmic heating powers $P_{NBI} = 2.5$ MW and $P_{ohm} = 0.3$ MW, respectively. The ELM frequency, $f_{ELM} \cong 40$ Hz and the energy lost per ELM, $\Delta W_{ELM} \cong 40$ kJ (corresponding to 9% of the plasma stored energy) were obtained from averaging over 21 ELMs.

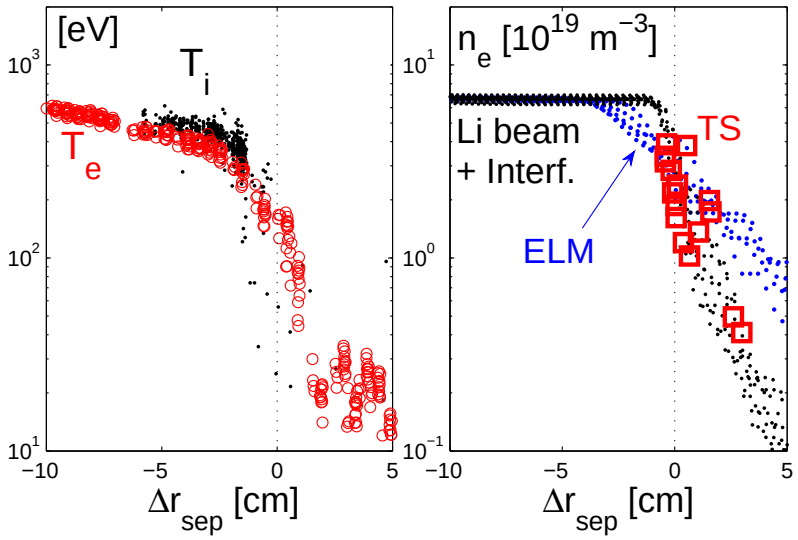

Figure 3. *Inter-ELM edge temperatures and electron density profiles during the RFA reciprocation. Left: T_e measured by the electron cyclotron emission diagnostic, T_i measured by the charge exchange recombination spectroscopy. Right: Electron density obtained from the Thomson scattering, lithium beam and the interferometer diagnostics. Also plotted is the edge density profile during the ELMs measured by the lithium beam and the interferometer diagnostics.*

The inter-ELM edge temperature and density profiles are plotted in figure 3. The separatrix parallel collisionality $\nu_e^* \approx q_{95}\pi R/\lambda_{ee} \approx 3$, where $\lambda_{ee} \approx 10^{16} T_e^2/n_e$ is the electron-electron collisional mean free path evaluated at the separatrix (with the temperature in electron volts as elsewhere in this paper). The RFA target position was 4.8 cm outside the separatrix. In this discharge, j_{sat} was not measured by the RFA slit plate. Measurements of j_{sat} were obtained in a series of similar discharges at $\Delta r_{sep} \geq 6$ cm.

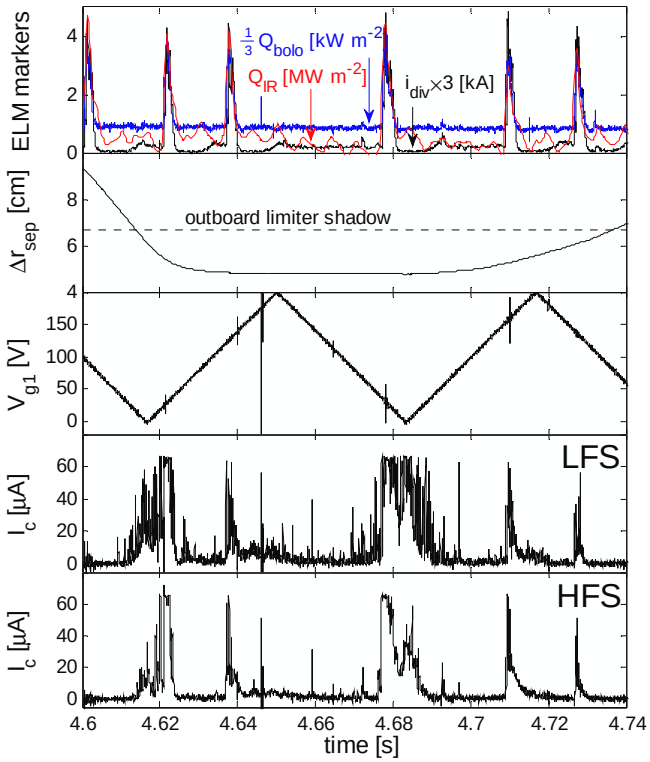

Figure 4. *From top to bottom: signal from the selected ELM markers (see text), RFA distance from the separatrix, voltage applied to the ion repelling RFA grid and the ion currents to the RFA collectors. LFS (HFS) indicates the analyzer intercepting magnetic field lines coming from the low field side (high field side). AUG discharge #25773.*

Figures 4 and 5 compile the time traces of I_c measured at both sides of the RFA. Also plotted in figure 4 are the time traces of Δr_{sep}, V_{g1}, and the selected ELM markers: the power density measured by a bolometric diode viewing the outer divertor Q_{bolo} (ϕ = 170°), the power density to the inner divertor measured by the infrared (IR) camera Q_{IR} (ϕ = 124°) and the total current to the inner divertor i_{div} measured with tile current monitor (ϕ = 10°). Poloidal location of these diagnostics is indicated in figure 1. Large bursts in I_c are synchronous with ELMs (ELMs recorded at $V_{g1} \approx 30$ V even saturate the collector signal so that the maximum amplitude of the ELM collector current, I_{cELM}, is not known). This alone provides clear evidence that the ELM ions reach the far SOL with the impact energies exceeding 160 eV ($V_{g1} = 160$ V being the highest bias voltage applied to grid 1 during any given ELM, table 1). At constant Δr_{sep}, I_{cELM} scales inversely with V_{g1}. This is seen clearly by comparing I_{cELM} measured at $\Delta r_{sep} = 4.8$ cm for $V_{g1} = 129$ and 26 V from figure 5 and table 1. At constant V_{g1}, I_{cELM} decreases with Δr_{sep} due to parallel losses to the divertor targets. The approximate e-folding length of the ELM ion impact energy is 2 cm (figure 5 and table 1). Almost no I_{cELM} is detected in the shadow of the outboard limiter at $\Delta r_{sep} = 9$ cm. In this region the parallel connection length L_{con} is shorter compared with the field line lengths in the main SOL, figure 6, so that the ELMs are quickly dissipated by enhanced parallel losses $\propto c_s / L_{con}$, with c_s the ion sound speed. The collector current is almost zero during the inter-ELM periods except at lowest V_{g1} when the "background" ions reach the collector, Sec. 2.4.

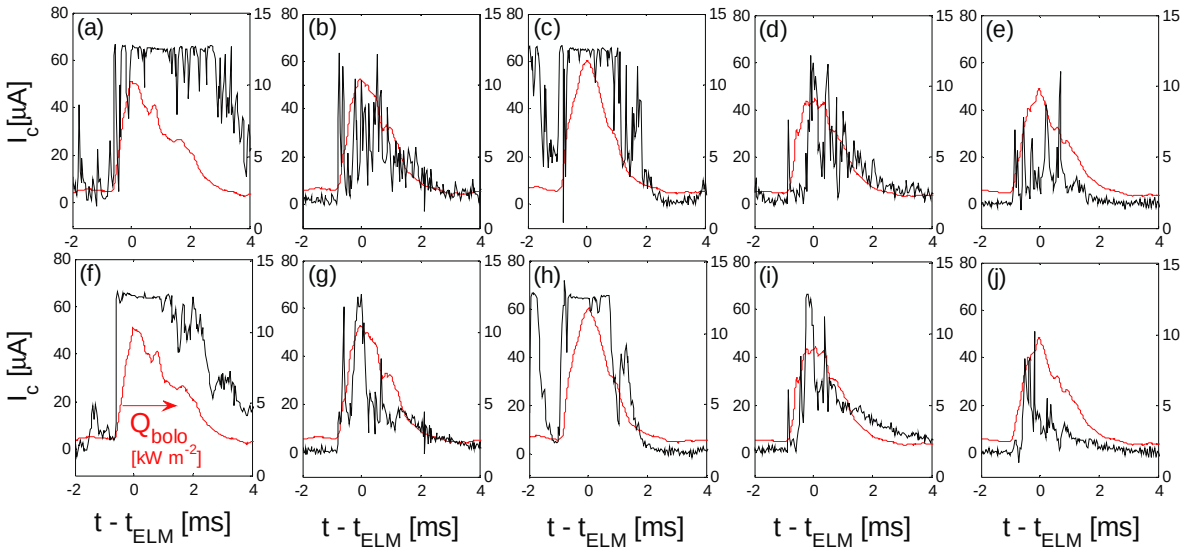

Figure 5. *Collector current measured during ELMs by the analyzer intercepting magnetic field lines coming from the low field side (top row) and the high field side (bottom row). Time is relative to* t_{ELM} *, defined here as a peak power density measured by the bolometric diode viewing the outer divertor,* Q_{bolo}*. The approximate values of the RFA distance from the separatrix and the voltage applied to the ion repelling grid during individual ELMs are stated in Table 1.*

Table 1. *From left to right: the RFA distance from the separatrix, the voltage applied to the ion repelling grid,* t_{ELM} *defined here as the ELM peak power density measured by the bolometric diode viewing the outer divertor* Q_{bolo}*, and the labelling used in figure 5.*

Δr_{sep} [cm]	V_{g1} [V]	t_{ELM} [s]	Label in figure 5
4.8	26	4.678	(a, f)
4.8	129	4.638	(b, g)
5.3	31	4.622	(c, h)
5.3	160	4.710	(d, i)
6.1	132	4.727	(e, j)

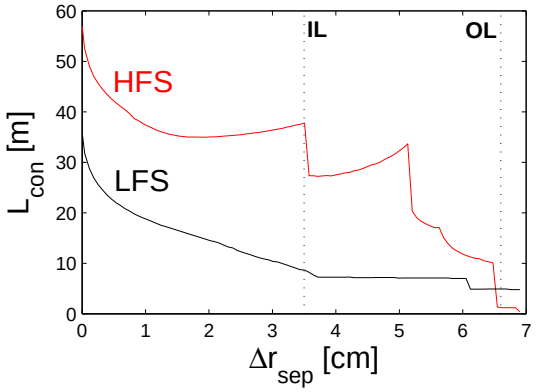

Figure 6. *Parallel connection length* L_{con} *during the RFA reciprocation in the discharge #25773, plotted against the distance from the separatrix.* L_{con} *is obtained from the magnetic field line tracing and equates to the length of the field line between the probe and the nearest surface. LFS (HFS) indicates the side of the probe intercepting the field lines coming from the low field side (high field side). Also indicated are the radii of the inboard and the outboard limiters. At* $\Delta r_{sep} \approx 5$ *cm the HFS connection jumps from the upper corner of the central column to the upper dump plates, leading to the abrupt decrease of the HFS* L_{con}*.*

Note that because of factor of ~2.7 wider slit on the HFS analyzer, the magnitude of I_{cELM} is similar on both sides of the RFA, even though j_{sat} measured during the ELMs, j_{satELM}, is strongly asymmetric with $j_{satELM}^{LFS} = 2-3\, j_{satELM}^{HFS}$, figure 7. The asymmetry in j_{satELM} can be interpreted as a plasma flow towards the LFS analyzer [19], and indicates that the ELM particles enter the SOL preferentially between the outer strike point and the RFA located above the outer midplane. This is consistent with the conclusion that the ELM plasma enters the SOL on the outboard side (e.g. [10, 20-23]). As illustrated in figure 8, similar ion current asymmetry (i.e. $j_{sat}^{LFS} > j_{sat}^{HFS}$) is observed also during the inter-ELM periods, though the ion current measured by the HFS slit plate is too low for estimating the far SOL inter-ELM plasma drift velocity.

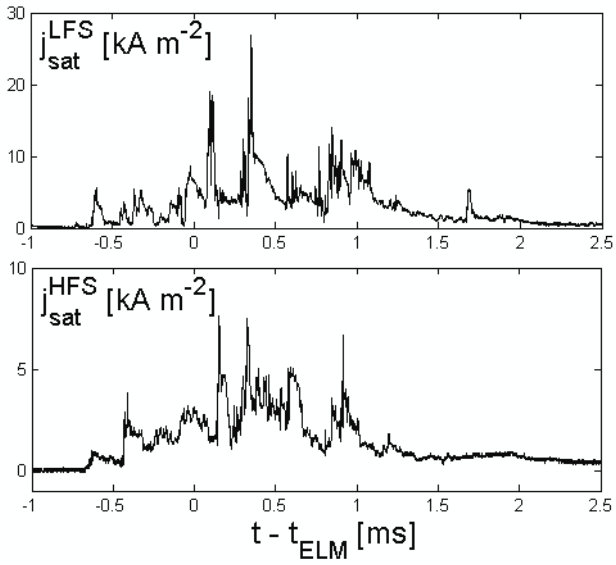

Figure 7. *Ion current density measured during an ELM by the RFA slit plates in the AUG discharge #25809, similar to #25773. RFA-separatrix distance $\Delta r_{sep} = 6.1$ cm. LFS (HFS) indicates the analyzer intercepting magnetic field lines coming from the low field side (high field side). t_{ELM} is defined here as a peak power density measured by the bolometric diode viewing the outer divertor during an ELM (Sec. 2.3).*

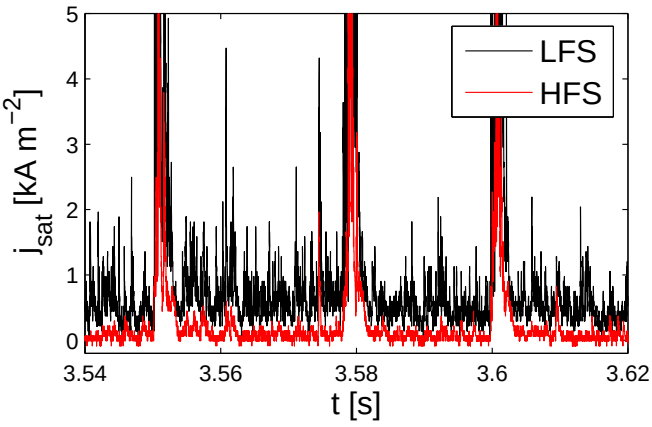

Figure 8. *Ion current density measured between ELMs by the RFA slit plates in the AUG discharge #25809, similar to #25773. RFA-separatrix distance $\Delta r_{sep} = 6.1$ cm. LFS (HFS) indicates the analyzer intercepting magnetic field lines coming from the low field side (high field side). Three large bursts of j_{sat} coincide with ELMs.*

Figures 5 and 7 show that $I_{c\,ELM}$ and $j_{sat\,ELM}$ consist of a number of time-separated current excursions. The same filamentary structure of an ELM has been observed in a number of tokamaks (e.g. [8, 10, 24, 25] and references in [2]) and reproduced by non-linear MHD models [21, 23]. We recall that $I_{c\,ELM}$ and $j_{sat\,ELM}$ were measured in the separate discharges and their response to individual ELM filaments cannot be compared directly. For the typical width and the separation of the large current filaments in AUG (both 100 – 200 μs [25]), only 3-6 data points are sampled on average per filament by the RFA collectors. As a result, some of the ELM filaments will be smeared out by the collector current measurement and the real amplitudes of the current excursions are not obtained, nor can any of the fine substructure in individual filaments, seen in measurements of $j_{sat\,ELM}$ and elsewhere (e.g. [8, 10, 24, 25]) be resolved.

2.3. ELM ion temperature in the far SOL

As mentioned earlier, $I_{c\,ELM}$ measured for a certain value of V_{g1} provides direct evidence that the ELM ions reach the far SOL with impact energies exceeding $Z_i e V_{g1}$. It is not clear, however, what fraction of the ELM ion energy distribution such ions represent. If the ELMs were measured by the RFA collector for a range of V_{g1}, a direct measurement of the ion energy distribution (and $T_{i\,ELM}$) could be obtained from the variation of $I_{c\,ELM}$ with V_{g1} (this is usually the standard output of an RFA operating in less transient conditions when events are not fast compared to the sweep voltage period). However, since the typical ELM rise time is much faster than the sweep period of V_{g1} in the present experiment, $I_{c\,ELM}$ is monitored at almost constant V_{g1}. The information about $T_{i\,ELM}$ thus cannot be obtained from the available measurements of V_{g1} and $I_{c\,ELM}$ alone.

Alternatively, $T_{i\,ELM}$ could be estimated for individual ELM filaments by comparing the ion currents measured simultaneously by the RFA collector at fixed V_{g1} and by the slit plate. Such analysis is, unfortunately, not possible here for individual ELM filaments since $I_{c\,ELM}$ and $j_{sat\,ELM}$ were measured in similar, but separate discharges. Therefore, in order to estimate $T_{i\,ELM}$ from the comparison of $I_{c\,ELM}$ and $j_{sat\,ELM}$, we will resort to the ELM-averaged quantities, which are insensitive to the differences in individual filaments as long as the ELMs are measured in similar pulses. This approach will allow us to compare $I_{c\,ELM}$ and $j_{sat\,ELM}$ measured for similar ELMs at $\Delta r_{sep} \cong 6.1\,\mathrm{cm}$ (which is the only radial position where both, $j_{sat\,ELM}$ and $I_{c\,ELM}$, are available), albeit in different pulses.

We define the average ELM collector current

$$\langle I_c \rangle_{ELM} = \Delta t_{ELM}^{-1} \int_{\Delta t_{ELM}} I_c dt\,, \tag{1}$$

where Δt_{ELM} is the ELM duration. Δt_{ELM} is arbitrarily defined as the time interval for which the intensity of the ELM marker, reduced by its mean inter-ELM value, is larger than $m_{peak}\exp(-1)$. $m_{peak} = m(t_{ELM})$ is the maximum intensity of the ELM marker for given ELM, reduced by its mean inter-ELM value. Δt_{ELM} evaluated for individual ELM markers from figure 4 varies less than 10%, meaning that Δt_{ELM} is almost independent of an ELM marker and the effect of different toroidal locations of the ELM marker measurements does not need to be considered. In our analysis, Δt_{ELM} is evaluated as a mean value of the ELM-markers Q_{bolo}, Q_{IR}, and i_{div}.

Because of high separatrix parallel collisionality noted in Sec. 2.2, the parallel velocity distribution of ELM ions $f(v_{//})_{ELM}$ is not expected to depart from thermal conditions. Therefore, we

assume Maxwellian $f(v_{//})_{ELM}$ with the characteristic temperature $T_{i\,ELM}$. Taking into account that all ions are accelerated in the sheath potential in front of the slit plate, the standard RFA model (e.g. [26]) gives

$$T_{i\,ELM} \cong \frac{V_{g1} - V_s}{\ln\left(\frac{\langle I_{c0}\rangle_{ELM}}{\langle I_c\rangle_{ELM}}\right)} \tag{2}$$

where $\langle I_c\rangle_{ELM}$ is measured at V_{g1} and

$$\langle I_{c0}\rangle_{ELM} \cong A_s \xi_r \xi_{opt}^3 \langle j_{sat}\rangle_{ELM}, \tag{3}$$

where $\langle I_{c0}\rangle_{ELM}$ is the average ELM collector current that would be measured at $V_{g1} = V_s$. At $V_{g1} = V_s$, no ions would be reflected by grid 1, Sec. 2.1, and the collector current would equal the ion current entering the RFA slit, multiplied by the total ion current transmission factor of the analyzer $\xi_r \xi_{opt}^3$. $\langle j_{sat}\rangle_{ELM}$ is obtained from $j_{sat\,ELM}$ in the same way as $\langle I_c\rangle_{ELM}$, Eq. (1). $A_s = h \times w$ is the slit area, Sec. 2.1. $A_s^{LFS} = 0.10$ mm^2 and $A_s^{HFS} = 0.28$ mm^2. The use of Eq. (3) is justified by the fact that ξ_r is a weak function of the parallel ion velocity and the grid transmission is optical independently of the grid bias voltage [13]. ξ_r is a function of the slit plate thickness relative to its width as well as the acceleration of ions in the Debye sheath in front of the slit plate relative to the ion temperature [13]. Since the latter is unknown and, at least in the L-mode plasmas, measured ξ_r deviates from the model predictions for a certain range of the parameter regimes, in Eq. (3) we assume for the LFS analyzer $\xi_r = 0.15 - 0.3$. This range encompasses most theoretical as well as experimental values of ξ_r for $w = 30\,\mu$m (which is very close to the LFS slit width) and 100–150 μm thick slit plate, measured by RFA in Tore Supra [13]. We recall, Sec. 2.1, that the slit plate mounted on the HFS analyzer has a factor of ~2.7 wider aperture for which the model for ξ_r predicts a factor of ~2 larger ξ_r. We thus assume $\xi_r = 0.3 - 0.6$ for the HFS analyzer.

At $\Delta r_{sep} = 6.1$ cm: $\left\langle j_{sat}^{LFS}\right\rangle_{ELM} \cong 5.6$ kA m^{-2}, $\left\langle j_{sat}^{HFS}\right\rangle_{ELM} \cong 2.9$ kA m^{-2}, $V_{g1} = 132$ V, $\left\langle I_c^{LFS}\right\rangle_{ELM} \cong 13.5\,\mu$A, $\left\langle I_c^{HFS}\right\rangle_{ELM} \cong 12.7\,\mu$A. Eq. (3) gives $\left\langle I_{c0}^{LFS}\right\rangle_{ELM} \cong 31 - 63\,\mu$A and $\left\langle I_{c0}^{HFS}\right\rangle_{ELM} \cong 91 - 182\,\mu$A. We assume $V_s = 40$ V (i.e. $\approx 2.7 T_{e\,ELM}$, with $T_{e\,ELM} \approx 15$ eV obtained previously by fast sweeping LP in the AUG far SOL [16]) for the sheath potential. Eq. (2) thus gives $T_{i\,ELM}^{LFS} \approx 60 - 111$ eV and $T_{i\,ELM}^{HFS} \approx 34 - 47$ eV.

Different effective ion temperatures on each side of a bi-directional RFA have been observed several times in L-mode plasmas (e.g. [27, 28]). The asymmetry is theoretically understood and is associated with the perturbing effect of the probe on the plasma, combined with the plasma flow [29]. The analyzer towards which the flow is directed (here the LFS analyser, Sec. 2.2) is expected to measure higher effective ion temperature [29]. The unperturbed ion temperature (namely that which would be observed in the absence of the probe) $T_{i\,ELM} \approx 50 - 80$ eV is given by averaging the HFS and the LFS measurements [29]. Note that in transient ELM conditions the parallel length from which the ELM ions are collected by the RFA ($c_s d / v_{r\,ELM} \approx 2 - 4$ m where $v_{r\,ELM}$ is the radial ELM filament propagation speed of which values for AUG far SOL are noted in the following section) is an order of magnitude longer than the cross-field probe dimension *d*, Sec. 2.1, which justifies the use of a simple one-dimensional parallel model from [29].

This RFA estimated value of $T_{i\,ELM}$ at $\Delta r_{sep} \cong 6.1\,\mathrm{cm}$ is in good agreement with $T_{i\,ELM} \approx 30-60\,\mathrm{eV}$ for $\Delta r_{sep} = 4-8\,\mathrm{cm}$, reported earlier from AUG [25] where $T_{i\,ELM}$ was estimated from comparison of $j_{sat\,ELM}$ measured by a simple LP and the heat flux density to the LP, monitored simultaneously by the fast IR camera. As pointed out in [25], the heat flux density was measured 5 mm behind the LP collectors, which could result in an underestimation of $T_{i\,ELM}$ by a factor of ~1.2 for the measured heat flux density e-folding length of 2.5 cm.

2.4. Inter-ELM ion temperature in the far SOL

As mentioned in Sec. 2.2 and seen in figures 4 and 9, at low values of V_{g1} the collector current increases during the inter-ELM periods with decreasing V_{g1}. Such current can be associated with "background" ions that are not fully repelled from the collector. Assuming, as for the ELM ions, that the parallel velocity distribution of the background ions is Maxwellian (which is very likely to be good approximation for high inter-ELM collisionalities in the far SOL $\nu_e^* \approx 10$ of the discharge #25773), the inter-ELM ion temperature T_i can be obtained from the slope of I_c measured during the inter-ELM period, plotted against V_{g1}, $I_c \propto \exp(-V_{g1}/T_i)$ (e.g. [26]). Figures 9 and 10 illustrate such analysis for I_c measured at $t \approx 4.685\,\mathrm{s}$ ($\Delta r_{sep} = 4.8\,\mathrm{cm}$). In order to ensure that the collector signal is not affected by the ELM appearing shortly before, the time interval from which I_c is included in the analysis begins when the signal of the ELM marker returns to the inter-ELM level. The current-voltage (I-V) characteristics – HFS and LFS collector currents plotted against V_{g1} – are shown in figure 10. The approximate values of ion temperatures obtained from the exponential fit to the decaying part of each characteristic are $T_i^{LFS} \approx 17\,\mathrm{eV}$ and $T_i^{HFS} \approx 8\,\mathrm{eV}$, with the unperturbed ion temperature ([29] and Sec. 2.3) $T_i = \left(T_i^{LFS} + T_i^{HFS}\right)/2 \approx 12\,\mathrm{eV}$. Within the accuracy of the measurements, T_i is comparable to the typical background electron temperature $T_e \approx 10\,\mathrm{eV}$, previously measured by the simple LPs in the AUG far SOL [17, 18]. The observation $T_i \approx T_e$ is consistent with relatively strong thermal coupling of ions and electrons; for given discharge parameters, the parallel ion transit time through the SOL $\tau_{//}^i \propto L_{con}/\sqrt{T_i + T_e} \approx 1.1\,\mathrm{ms}$ is roughly equal to the ion-electron thermalization time: $\tau_{th}^{ie} \propto T_e^{3/2}/n_e \approx 1.4\,\mathrm{ms}$. The ions and electrons are, therefore, expected to have similar temperatures.

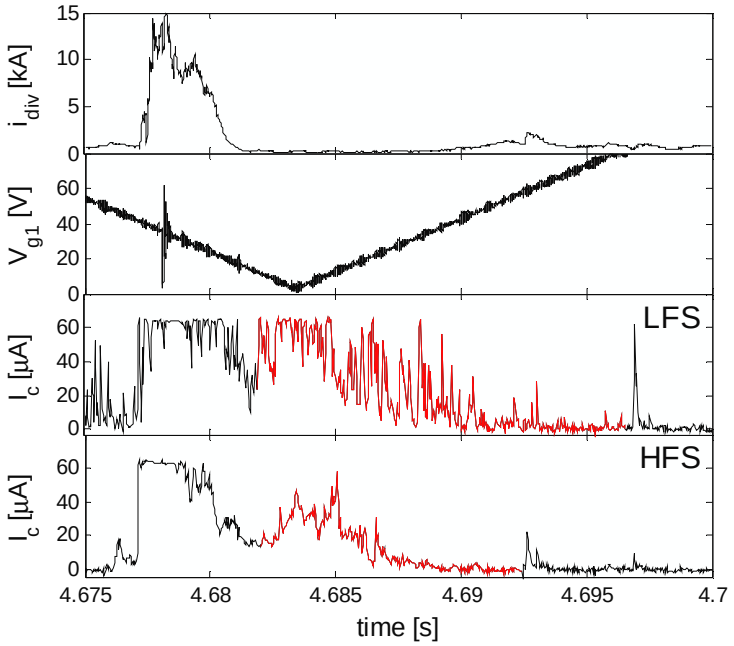

Figure 9. *From top to bottom: total current to the inner divertor i_{div} (chosen as ELM marker), voltage applied to grid 1, ion currents measured by the RFA collectors. The portion of the I_c traces highlighted in red corresponds to the fraction of the ELM cycle from which the inter-ELM ion temperatures in figure 10 are estimated. LFS (HFS) indicates the analyzer intercepting magnetic field lines coming from the low field side (high field side).*

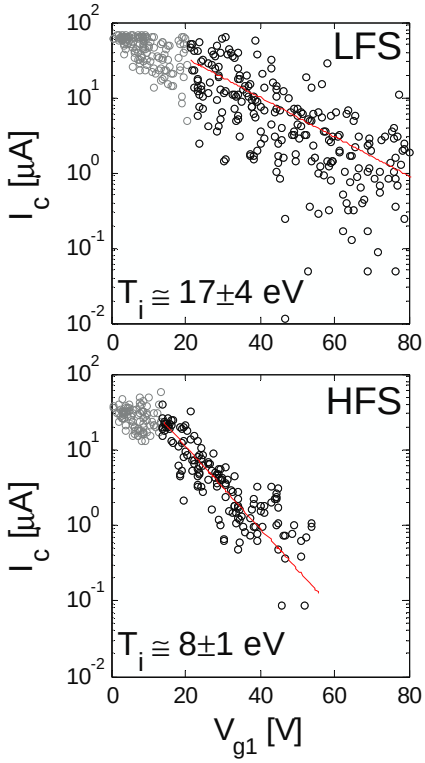

Figure 10. *Current-voltage (I-V) characteristics measured by the RFA during the inter-ELM period $t \cong 4.685$ s, $\Delta r_{sep} = 4.8$ cm, AUG discharge #25773). Collector current is plotted against the voltage applied to ion repelling grid 1. I_c is measured during the inter-ELM period highlighted in figure 9. Also noted are the ion temperatures obtained from the exponential fit (full line) to the decaying part of the I-V characteristic (black circles). LFS (HFS) indicates the analyzer intercepting magnetic field lines coming from the low field side (high field side).*

3. $T_{i\,ELM}$: measurements versus modeling

This section compares the ELM ion temperature estimated from the AUG RFA measurements with the predictions of two models, referred to, for simplicity as the "fluid" (though a kinetic equivalent also exists) [2, 12] and the "kinetic" [3, 30, 31, 32]. Roughly speaking, in both models, the quantity of particles and energy carried by ELM filaments into the far SOL is determined by the competition between the parallel losses to the targets and the filament propagation across the SOL with a specified $v_{r\,ELM}$. A good match has previously been achieved between the fluid model and the RFA measurements of the ELM filament ion current densities in the JET far SOL [2, 10, 12]. The kinetic model has been successful in reproducing the ELM divertor heat load profiles in both MAST [30] and AUG [31]. Both models also predict similar $T_{i\,ELM}$ in the far SOL of the ITER reference scenario (260–420 eV from the fluid model [2] and 200–500 eV from the kinetic model [3], assuming $v_{r\,ELM} = 350 - 600$ and $500 - 1000$ m s^{-1}, respectively).

In the fluid model, the ELM filament propagation across the SOL is described in the filament frame by the temporal evolution of a Gaussian wave packet in which the initial particle and energy content decreases due to parallel losses to the divertor targets [2, 12]. The radial distance and the time of the filament propagation are related by $v_{r\,ELM}$. Ion and electron fluids are coupled through the equipartition term. Current understanding of the ELM cycle is insufficient to provide theory-based estimates for the position at which any given ELM filament seen in the SOL originates. To account for this uncertainty, we have calculated the radial profiles of $T_{i\,ELM}$ for two different sets of initial conditions: a filament released (i) from the pedestal top ($\Delta r_{sep} = -2$ cm) with $T_{i\,ped} = T_{e\,ped} = 400$ eV and $n_{e\,ped} = 6 \cdot 10^{19}$ m^{-3} and (ii) from the separatrix with $T_{i\,sep} = T_{e\,sep} = 150$ eV and $n_{e\,sep} = 3 \cdot 10^{19}$ m^{-3} (figure 3). The parallel system size is determined by L_{con}, figure 6. High parallel separatrix collisionality of the discharge #25773, estimated in Sec. 2.2, justifies the use of the fluid description.

The kinetic simulation begins by distributing ions uniformly along L_{con} into a number of filaments, each containing 10^6 ions. The initial ion velocity distribution is Maxwellian with the temperature $T_{i\,ped} = 400$ eV. The trajectory of each ion, propagating across the SOL with radial velocity $v_{r\,ELM}$, is followed until it intersects the wall or divertor plates. For each radial position, $T_{i\,ELM}$ is obtained from the local ion velocity distribution. The electrons are not included in the simulation, assuming that they lose their energy much faster than ions because of much higher electron parallel heat conductivity. A sensitivity study with the fluid model showed that the thermal coupling of ELM ion and electron fluids has almost no effect on $T_{i\,ELM}$ for the plasma parameter regime considered here.

Both models require $v_{r\,ELM}$ as input. A value of $v_{r\,ELM} = 1500$ m s^{-1} has been assumed here, corresponding to the maximum of the probability distribution function of $v_{r\,ELM}$ in the far SOL of AUG measured for a broad range of the plasma parameters [3, 32]. $v_{r\,ELM}$ were obtained by the so called filament probe [3, 32, 33], considered to be currently the most reliable diagnostic for $v_{r\,ELM}$ measurements [32]. To test the sensitivity of the predicted $T_{i\,ELM}$ to $v_{r\,ELM}$ (a range of $v_{r\,ELM} = 300 - 3500$ m s^{-1} has been reported for the AUG far SOL [32]), both the kinetic and fluid simulations were executed also for $v_{r\,ELM} = 1000$ and 2000 m s^{-1}. Due to the lack of $v_{r\,ELM}$ measurements in the near SOL, we assume that $v_{r\,ELM}$ is radially constant in the SOL, though the ELM filaments have to accelerate in the near SOL [32].

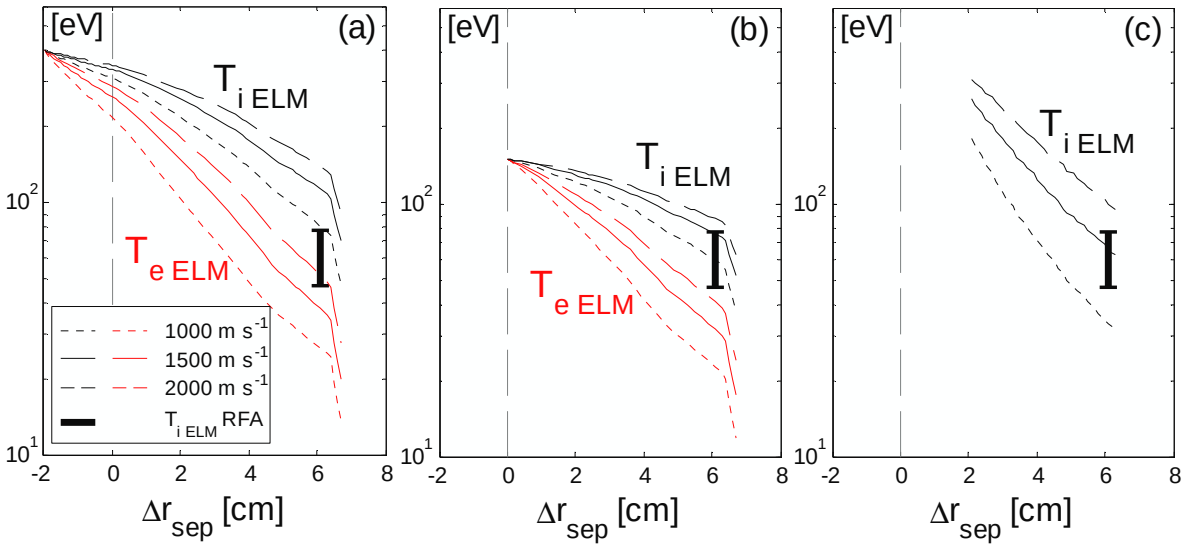

Figure 11. *ELM ion temperature $T_{i\,ELM}$ estimated from the RFA measurements (vertical bar) compared with model predictions. Temperatures are plotted against the distance from the separatrix. (a) Fluid model, ELM filament launched from the pedestal top, (b) fluid model, ELM filament launched from the separatrix, (c) the kinetic model. Radial ELM propagation speed $v_{r\,ELM}$ = 1000 (dotted) 1500 (full) and 2000 m s^{-1} (dashed).*

In figure 11, $T_{i\,ELM}$ estimated from the RFA data is compared with model predictions. Both the fluid and kinetic approaches predict a similar range of $T_{i\,ELM}$, which can be easily understood, given the high ν_e^*. The fluid model result is closer to the experimental value for the ELM filament released from the separatrix rather than the pedestal top. Sharp drop of both temperatures in the shadow of the outboard limiter (i.e. $\Delta r_{sep} > 6.5$ cm) in the fluid simulations is due to shorter L_{con} and agrees qualitatively with very low $I_{c\,ELM}$ measured by RFA in that region (figure 4). Good agreement is also achieved with the far SOL $T_{i\,ELM}$ predicted by the kinetic model. However, the simulation results have to be considered within the bounds of the assumptions on $v_{r\,ELM}$ to which both models are sensitive. For example, if $v_{r\,ELM}$ assumed in the simulations would increase radially in the near SOL to the value measured in the far SOL, lower ELM temperatures would be obtained in the far SOL. Consequently, better match could be obtained between the RFA measurements and the fluid model for the ELM filament launched from the pedestal top rather than the separatrix. In fact, this would be consistent with the observation that the electron density measured during ELMs by simple Langmuir probes in the far SOL of AUG is a substantial fraction of $n_{e\,ped}$ [16]. Finally, the finding $T_{i\,ELM} > T_{e\,ELM}$ from the fluid model is consistent with ELM kinetic modelling [8] and can be explained by higher parallel losses of electrons because of their higher mobility.

4. Summary

Transient heat loads to the first wall during ELMs is an important issue for the ITER burning plasma operation. They depend strongly on energies carried by ELM ions to the first wall. The measurements of ELM ion energies in the far SOL (i.e. near the first wall radius) are, however, very sporadic [10, 11, 25]. Sparse experimental data for testing the models is a major reason why the predictions of the ELM-wall interaction in ITER are associated with large uncertainties.

This paper describes first measurements of the ELM ion energies in AUG far SOL using a RFA. During type-I ELMs, ion impact energies of at least 160 eV have been measured at the distance 5–6 cm outside the separatrix. This alone provides further evidence that ELM ions can reach the far

SOL with a significant fraction of the pedestal energies, confirming earlier observations [5, 10, 11, 25]. The radial decay length of $E_{i\,ELM} \approx 2\,\mathrm{cm}$. At $\Delta r_{sep} \cong 6\,\mathrm{cm}$, the average ELM-filament ion temperature estimated from the RFA measurements is in the range $50-80\,\mathrm{eV}$. The inter-ELM ion temperature in the far SOL was found to be substantially lower ($T_i \approx 12\,\mathrm{eV}$) and comparable to the inter-ELM electron temperature, which is consistent with a high degree of inter-ELM ion-electron thermal coupling in the discharges studied.

The experimentally measured $T_{i\,ELM}$ can be reasonably well reproduced by two different models of the ELM parallel transport in the SOL, increasing thus the confidence of the model predictions of the ELM-wall interaction in ITER. There is, however, substantial uncertainty in the model predictions because of uncertainty in the parameters to which the models are sensitive (such as radial propagation speed and the radial location from which the ELM filaments are released into the SOL).

Acknowledgements
The authors are grateful to W. Fundamenski and D. Moulton from JET for providing access to the fluid parallel loss simulator and to the Association Euratom - CEA for supporting this experiment.

References

[1] Pitts R A *et al* 2010 Physics basis and design of the ITER plasma-facing components *J. Nucl. Mater.* (to be published)
[2] Fundamenski W, Pitts R A and JET EFDA Contributors 2006 *Plasma Phys and Control. Fusion* **48** 109
[3] Kirk A, Lisgo S, Nardon E, Eich T, Herrmann A, Kallenbach A and Loarte A 2009 *J. Nucl. Mater.* **390-391** 727
[4] Herrmann A, Eich T, Rohde V, Fuchs C J, Neuhauser J and ASDEX Upgrade team 2003 *Proc. 30th EPS Conf. On Contr. Fusion and Plasma Phys. (St. Petersburg, 7-11 July 2003)* vol **27A**(ECA) p P-1.155.
[5] Herrmann A, Eich T, Rohde V, Fuchs C J, Neuhauser J and ASDEX Upgrade team 2004 *Plasma Phys. Control. Fusion* **46** 971
[6] Herrmann A, Neuhauser J, Rohde V, Dux R, Eich T, Fuchs C J, Ye M Y and ASDEX Upgrade team 2005 *J. Nucl. Mater.* **337-339** 697
[7] Arnoux G *et al* 2007 *Proc. 34th EPS Conference on Plasma Phys. (Warsaw, 2 - 6 July 2007)* vol **31F**(ECA) p P-1.023
[8] Pitts R A, Andrew P, Arnoux G, Eich T, Fundamenski W, Huber A, Silva C, Tskhakaya D and JET EFDA Contributors 2007 *Nucl. Fusion* **47** 1437
[9] Dux R, Herrmann A, Kallenbach A, Neu R, Neuhauser J, Maier H, Pugno R, Pütterich T, Rohde V and ASDEX Upgrade Team 2007 *J. Nucl. Mater.* **363-365** 112
[10] Pitts R A, Fundamenski W, Erents S K, Andrew Y, Loarte A, Silva C and JET-EFDA contributors 2006 *Nucl. Fusion* **46** 82
[11] Tamain P, Kočan M, Kirk A, Gunn J P, Pascal J-Y and Price M 2010 Ion energy measurements in the scrape-off-layer of MAST using a retarding field analyzer *J. Nucl. Mater.* (to be published)
[12] Fundamenski W, Pitts R A and JET EFDA Contributors 2007 *J. Nucl. Mater.* **363-365** 319
[13] Kočan M, Gunn J P, Komm M, Pascal J-Y, Gauthier E, and Bonhomme G 2008 *Rev Sci. Instrum.* **79** 073502
[14] Kočan M 2009 *PhD Thesis* Nancy-Université
[15] Guo H Y, Matthews G F, Davies S J, Erents S K, Horton L D, Mond R D and Stangeby P C 1996 *Contrib. Plasma Phys.* **36** 81
[16] Müller H W *et al* 2011 Fluctuations, ELM filaments and turbulent transport in the SOL at the outer mid plane of ASDEX Upgrade *Nucl. Fusion* (submitted)
[17] Müller H W *et al* 2010 *Contrib. Plasma Phys.* **50** 847
[18] Horaček J *et al* 2010 *Nucl. Fusion* **50** 105001
[19] Hutchinson I H 1991 *Phys. Fluids B* **3** 847
[20] Gonçalves B, Hidalgo C, Pedrosa M A, Silva C, Balbín R, Erents S K, Hron M, Loarte A and Matthews G F 2003 *Plasma Phys. Control. Fusion* **45** 1627

[21] Snyder P B and Wilson H R 2003 *Plasma Phys. Control. Fusion* **45** 1671
[22] Boedo J A *et al* 2005 *Phys. Plasmas* **12** 072516
[23] Huysmans G T A, Pamela S, van der Plas E and Ramet P 2009 *Plasma Phys. Control. Fusion* **51** 124012
[24] Silva C, Gonçalves B, Hidalgo C, Erents S K, Loarte A, Matthews G F, Pedrosa M 2005 *J. Nucl. Mater.* **337-339** 722
[25] Herrmann A *et al* 2007 *J. Nucl. Mater.* **363-365** 528
[26] Wan A S, Yang T F, Lipschultz B and LaBombard B 1986 *Rev. Sci. Instrum.* **57** 1542
[27] Pitts R A *et al* 2003 Proc. *Proc. 30th EPS Conf. On Contr. Fusion and Plasma Phys. (St. Petersburg, 7-11 July 2003)* vol **27A**(ECA) p P-2.84
[28] Kočan M and Gunn J P 2009 *Proc. 36th EPS Conference on Plasma Phys. (Sofia, June 29 - July 3)* vol **33E**(ECA) p P-4.203.
[29] Valsaque F, Manfredi G, Gunn J P and Gauthier E 2002 *Phys. Plasmas* **9** 1806
[30] Kirk A *et al* 2007 *Plasma Phys. Control. Fusion* **49** 1259
[31] Kirk A *et al* 2008 *J. Phys.: Conf. Ser.* **123** 012012
[32] Kirk A *et al* 2011 Parameters determining the radial propagation of type-I ELMs in ASDEX Upgrade *Plasma Phys. Control. Fusion* (in press)
[33] Schmid A, Herrmann A, Müller H W and the ASDEX Upgrade Team 2008 *Plasma Phys. Control Fusion* **50** 045007